Experimental Observation of Topologically Protected Bound States with Vanishing Chern Numbers in a Two-Dimensional Quantum Walk

Bo Wang,[*] Tian Chen,[*,†] and Xiangdong Zhang[‡]
Beijing Key Laboratory of Nanophotonics & Ultrafine Optoelectronic Systems, School of Physics, Beijing Institute of Technology, 100081 Beijing, China

(Received 30 April 2018; published 6 September 2018)

Quantum walks (QWs) provide a powerful tool as a quantum simulator to study and understand topological phases. Using such a quantum simulator, some topological phenomena have been discussed. However, all the experimental observations on the topological phenomena in QWs have been restricted to evolution in one dimension (1D) so far. The existing 2D experimental platforms cannot be applied to study topological phenomena due to lack of full control in the position space. Thus, some interesting topological phenomena in the 2D QW that do not exist in the 1D case, e.g., the edge-state-enhanced transport, have not been demonstrated experimentally. Here we report the experimental realization of 2D QW using spatial positions and orbital angular momentum of light. Based on our constructed experimental platform, we have observed 2D topological bound states with vanishing Chern numbers and confirmed the robustness of these bound states with respect to perturbations and disorder, which go beyond what has been known in static systems and are unique to periodically driven systems. Our studies not only represent an important advance in the study of topological phases, but also open up an avenue to explore topological properties in multidimensional QWs.

DOI: 10.1103/PhysRevLett.121.100501

Topological phases exhibit some most striking phenomena in modern physics. A prominent feature of a topological phase is the emergence of topologically protected edge states, which are robust against local perturbations and play a crucial role in the topological functionality of the underlying system [1–7]. Such a phenomenon has been extensively studied in condensed matter physics such as the quantum Hall effect and the quantum spin Hall effect, topological insulators, and topological superconductors [8–11]. Topological phases of the system can be classified by standard topological invariants, such as Chern numbers [12,13]. Recently, anomalous topologically protected edge states have been shown in propagating waveguide arrays with different Floquet orders [14–20].

On the other hand, recent investigations have also shown that quantum walks (QWs) can not only provide a versatile platform for studying static topological phases but also give unique opportunity to study topological phenomena in driven systems [21–38]. Based on such a platform, topologically protected pairs of nondegenerate bound states, topological quantum transitions, and topological invariants have been observed experimentally [26,31–37]. However, all these observations have been restricted to evolution in one dimension (1D). Some theoretical investigations have shown that 2D QWs can exhibit much richer topological phenomena than 1D QWs, e.g., the edge-state-enhanced transport in the 2D QW [38,39]. To observe these phenomena, an adequate control of positions in the 2D QW is required. Although 2D QWs have been experimentally realized in optical fiber networks, 2D waveguide arrays and photons [40–44], the positions in these systems cannot be fully controlled. Thus, the topological phenomena in 2D QWs cannot be observed based on these experimental platforms.

Here we construct a new 2D QW platform in which spatial positions and orbital angular momentum (OAM) states of light serve as two distinct degrees of freedom in the position space of 2D QWs. In the experiment, we employ a customized q plate involving multiple patterns to match the parallel multibeams produced by beam displacers (BDs), then construct inhomogeneous regions in 2D QWs by applying different coin operators to the beams in different spatial positions. Topologically protected bound states can be formed at the boundary between these inhomogeneous regions. Especially, we observe topologically protected bound states with vanishing Chern numbers, which go beyond what has been known in static systems and is unique to the periodically driven systems. As the first experiment to observe topological phases in the 2D QW, our work opens up an avenue to study topological properties in multidimensional QWs.

Experimental realization of the 2D quantum walk.—Our experimental setup to perform the 2D QW is illustrated in Fig. 1, which consists of three modules: Fig. 1(a), state preparation; Fig. 1(b), many steps of 2D QW; Fig. 1(c), detection. In our experimental scheme, the coin of 2D QW is encoded by the polarization, and the 2D lattice is mapped to a grid implemented by the OAM states and spatial

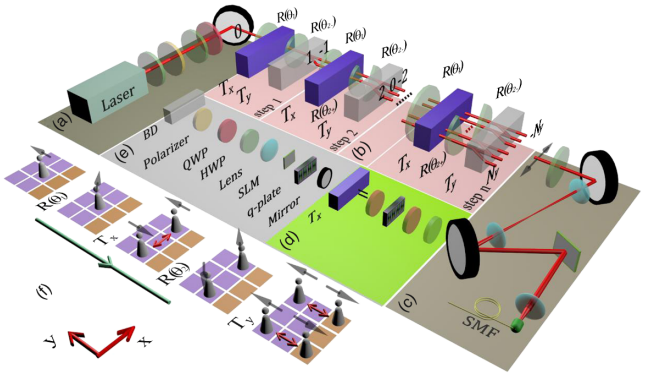

FIG. 1. Experimental scheme for 2D QWs. (a) State preparation. (b) Many steps of 2D QW. In our study of probing topological properties in 2D QWs, we create spatially inhomogeneous rotations in regions $-N_y < y < 0$ and $0 \le y < N_y$, which are realized by semicircular HWPs $R(\theta_{2,+})$ and $R(\theta_{2,-})$ in (b). (c) Detection. (d) T_x. (e) The list of all optical devices. (f) The schematic representation of first step in a 2D QW. Rotation angles: purple region, $R(\theta_1)$, $R(\theta_{2,+})$; yellow region, $R(\theta_1)$, $R(\theta_{2,-})$.

positions of the beam. Here, we use the classical light source (from a 632.8 nm helium-neon laser) instead of a single photon source to perform experiments, since the previous investigations have shown that the QW can be implemented using an entirely classical light source due to the similarity between coherent processes in quantum mechanics and classical optics [40,45]. One step operator of the 2D QW is described as

$$U = T_y R(\theta_2) T_x R(\theta_1), \tag{1}$$

where $R(\theta_{1(2)}) = e^{-i\theta_{1(2)}\sigma_y/2}\sigma_z$ is a coin operator, which is realized by one HWP on the polarization of the beam in our experiment [see $R(\theta_1)$ and $R(\theta_2)$ in Fig. 1(b)]. Here σ_y and σ_z are Pauli operators in the y and z directions, respectively. The parameter $\theta_{1(2)}$ represents the rotation angle of HWP. In Eq. (1), $T_x = \sum_x |x+1\rangle\langle x| \otimes |H\rangle\langle H| + |x-1\rangle\langle x| \otimes |V\rangle\langle V|$ represents the conditional shift operator along the x direction. We use different OAM states of beam to represent different sites x, $|H\rangle$, and $|V\rangle$ stand for the horizontal and vertical polarization of the beam, respectively. The operator T_x can be realized by shifting the OAM state depending on the current polarization of beam, and the optical elements to realize T_x are addressed in Fig. 1(d).

In the experiment, we use BDs to realize the conditional shift operator $T_y = \sum_y |y+1\rangle\langle y| \otimes |H\rangle\langle H| + |y-1\rangle\langle y| \otimes |V\rangle\langle V|$. Different output spatial positions on the lateral section of BD are used to represent different sites y in the 2D QW [26,42,46,47]. The optical realizations of T_x and T_y are given in the Supplemental Material (SI) [48].

As presented in the experiment [see Fig. 1(b)], we use two semicircular HWPs $R(\theta_{2,+})$ and $R(\theta_{2,-})$ to work on beams whose spatial positions belong to $0 \le y < N_y$ and $-N_y < y < 0$, respectively. When the input beam enters the module [Fig. 1(b)], it undergoes the operations $R(\theta_1)$, T_x, $R(\theta_2)$, and T_y one by one in step 1. Such a process is described schematically in Fig. 1(f). The coordinates x and y in the 2D $x-y$ plane of Fig. 1(f) are mapped from OAM states and spatial positions of the beam, respectively. Because of the conditional movements along the x and y directions with T_x and T_y, the 2D walker emerges at four different sites with certain probabilities [see Fig. 1(f)] after the first step of 2D QW is completed. To undergo N steps of 2D QW, we experimentally repeat the above series of operations N times on the input beam; see Fig. 1(b). Then, the beams transport into the detection module in Fig. 1(c). Details of detection are addressed in the Supplemental Material (SI) [48].

In Figs. 2(a)–2(c), we provide experimental probability distributions at the fourth step in a homogeneous 2D QW. The results for other steps ($n \le 3$) are provided in the Supplemental Material (SII) [48]. The similarity $S[P_{\rm th}(x,y), P_{\rm ex}(x,y)] = (\sum_{x,y=-N}^{N} \sqrt{P_{\rm th}(x,y)P_{\rm ex}(x,y)})^2$ is presented to evaluate the quality of experiment. Here $P_{\rm th}(x,y)$ $[P_{\rm ex}(x,y)]$ represents the theoretical [experimental] probability distribution in the 2D QW. When the experimental result is close to the theoretic result, the value of S approaches 1.

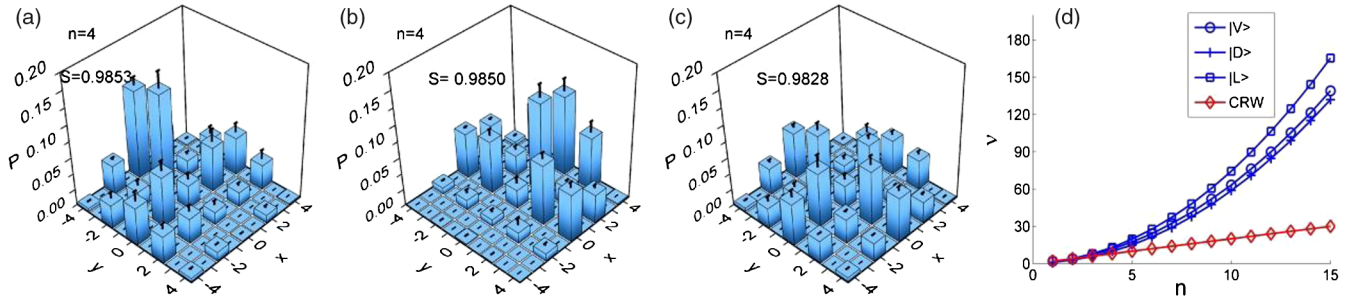

FIG. 2. (a)–(c) Experimental probability distributions in a homogeneous 2D QW at the fourth step. The walker starts from the lattice site (0,0) and rotation angles are $\theta_1 = \theta_{2,+} = \theta_{2,-} = (\pi/2)$. Error bars indicate the standard deviation. The initial polarizations of light are (a)$|V\rangle$, (b) $|D\rangle = 1/\sqrt{2}(|H\rangle + |V\rangle)$, (c) $|L\rangle = 1/\sqrt{2}(|H\rangle + i|V\rangle)$. (d) The variances between 2D QWs and CRW with steps.

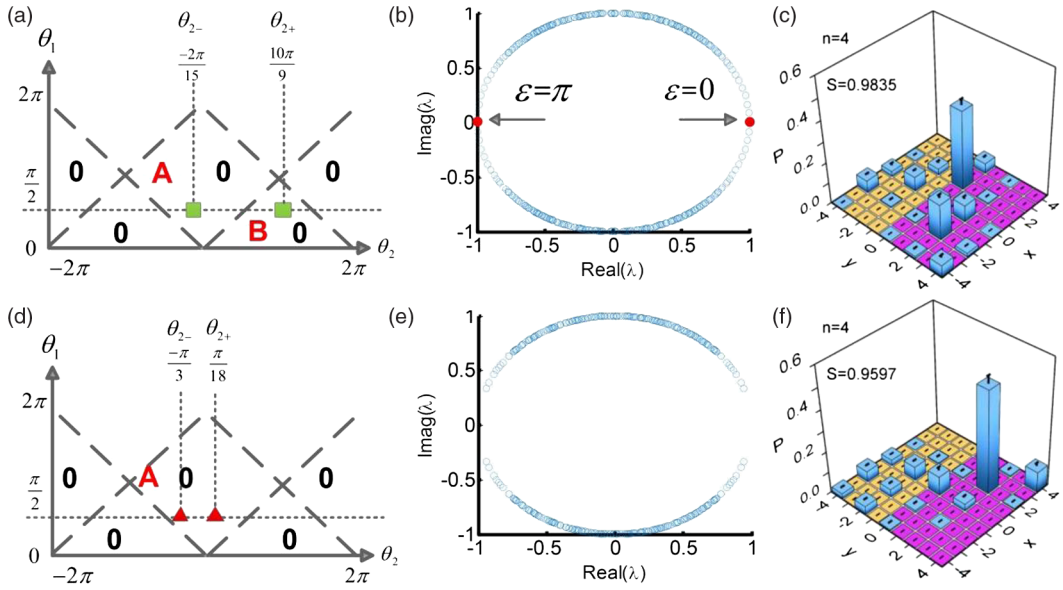

FIG. 3. (a)–(c) Experimental observations of bound states. (a) The phase diagram for 2D QW. Green squares in A ($\theta_1 = (\pi/2)$, $\theta_{2,-} = -(2\pi/15)$) and B ($\theta_1 = (\pi/2)$, $\theta_{2,+} = (10/9)\pi$) represent rotation angles of coin operators used in (b) and (c). (b) The eigenvalues $\lambda = e^{-i\varepsilon}$ of U. Red dots indicate $\varepsilon = 0$ and $\varepsilon = \pi$ energy bound states. (c) Measured probability distribution at the fourth step. (d)–(f) Experimental observations of no bound states. (d) The phase diagram for 2D QW. Red triangles represent rotation angles of coin operators in (e) and (f). Left ($\theta_1 = (\pi/2)$, $\theta_{2,-} = -(\pi/3)$); right ($\theta_1 = (\pi/2)$, $\theta_{2,+} = (\pi/18)$). (e) The eigenvalues $\lambda = e^{-i\varepsilon}$ of U. (f) Measured probability distribution at the fourth step. In (c) and (f), the walker starts from the lattice site (0,0), and the initial polarization of light is $|H\rangle$. Error bars indicate the standard deviation.

From Figs. 2(a)–2(c), we find that mean positions $(\bar{x}, \bar{y})_{\text{ex}} = \sum_{x,y}(x, y)P_{\text{ex}}(x, y)$ for these probability distributions are $(\bar{x}, \bar{y})_{\text{ex}} = (0.30, 0.41)$, $(-1.04, -0.09)$, and $(-0.04, 1.6)$, which are different from classical random walks (CRW) with the mean position (0,0). To better illustrate the difference between QWs and CRW, we theoretically provide the variances in Fig. 2(d). The variance is defined as $v = \sum_{x,y} P_{\text{th}}(x,y)|(x,y) - (\bar{x},\bar{y})_{\text{th}}|^2$ with the theoretical mean position $(\bar{x}, \bar{y})_{\text{th}} = \sum_{x,y}$ $(x, y)P_{\text{th}}(x, y)$. The variances for 2D QWs with initial polarizations $|V\rangle$, $|D\rangle = 1/\sqrt{2}(|H\rangle + |V\rangle)$ and $|L\rangle = 1/$ $\sqrt{2}(|H\rangle + i|V\rangle)$ are addressed as blue circles, dots, and rectangles in Fig. 2(d). The variance for CRW is presented as red diamonds for comparison. The variances increasing *quadratically* with steps display the ballistic spreading of QWs. In contrast, the variance in CRW grows *linearly* with steps. Since the variance is closely related to the probability distribution, we can obtain the values of variances for experimentally measured probability distributions; e.g., in Figs. 2(a)–2(c), the values of variances are 10.9, 9.6, and 12.0. However, the variance for CRW at the fourth step is 8. This means that 2D QWs have indeed been achieved in our experiments.

Experimental observation of topologically protected bound states with vanishing Chern numbers.—To observe topological bound states in 2D QWs, we need to create spatially inhomogeneous regions in the walk, which cannot be realized in the previous experimental platforms [40–44]. Here, as addressed in Fig. 1(b), an inhomogeneous 2D QW can be realized by applying different coin operators $R(\theta_{2,+})$ and $R(\theta_{2,-})$ to spatial positions $0 \le y < N_y$ and $-N_y < y < 0$. A boundary between the purple region and yellow region shown in Fig. 1(f) can be constructed. Figure 3(c) shows experimental probability distribution at the fourth step in 2D lattice sites. The corresponding probability distributions at other steps are given in the Supplemental Material (SV) [48].

From Fig. 3(c), it is clearly seen that large localized probability distribution appears along the boundary even at the fourth step, which hints at the emergence of bound states. According to the topology theory, bound states exist at the boundary between two regions governed by Hamiltonians with different Chern numbers [1–3,12, 13,38]. In order to further analyze the above phenomenon, we plot the phase diagram described by the Chern number for different θ_1 and θ_2 in Fig. 3(a). The calculations of Chern numbers in the 2D QW have been addressed in Secs. SIII and SIV of Supplemental Material [48]. The rotation angles of coin operators $(\theta_1, \theta_{2,-})$ and $(\theta_1, \theta_{2,+})$ in the experiment [results shown in Fig. 3(c)] are marked as green squares in Fig. 3(a). When the rotation angles change continuously from $(\theta_1, \theta_{2,+})$ to $(\theta_1, \theta_{2,-})$, the 2D QW needs to cross the gapless phases addressed as dashed lines. In Fig. 3(b), we provide the corresponding eigenvalues $\lambda = e^{-i\varepsilon}$ of U. We find that the bound states with $\varepsilon = 0$ and $\varepsilon = \pi$ emerge at the boundary between regions with two zero Chern number phases. In this case, the emergence of

bound states cannot be fully characterized by Chern numbers, and the bulk-boundary correspondence theorem is not satisfied [2].

For comparison, we choose coin rotations $(\theta_1, \theta_{2,+})$ and $(\theta_1, \theta_{2,-})$ of U located in the same region A of the phase diagram [Fig. 3(d)] and study the topological phenomena with such operator U. In this case, when rotation angles change continuously from $(\theta_1, \theta_{2,+})$ to $(\theta_1, \theta_{2,-})$, the effective Hamiltonian of QW is always gapped without crossing the gapless phase. The corresponding eigenvalues $\lambda = e^{-i\varepsilon}$ of U are shown in Fig. 3(e) and bound states cannot be found. In Fig. 3(f), we present experimental probability distribution in this 2D QW. The initial settings of the input beam are identical with those in Fig. 3(c). However, the phenomenon is completely different. In the present case, the probability along the boundary between the purple and yellow regions decreases quickly as the step increases, which reveals that there are no bound states in the present 2D QW.

The above phenomenon can be described very well by localized probabilities at the boundary P_{bound}. Here P_{bound} is defined as $P_{\text{bound}} = P(y = 0) + P(y = -1)$, $P(y = 0)$, and $P(y = -1)$ are marginal probabilities along $y = 0$ and $y = -1$ in 2D QW, respectively. In Fig. 4(a), we provide localized probabilities with step. Black squares and red circles represent theoretical and experimental results for the case in Fig. 3(a)–3(c). We find that P_{bound} always keeps a large value with the increase of steps. In contrast, for the case without bound states in Fig. 3(d)–3(f), P_{bound} decreases to a small value ($P_{\text{bound}} \leq 0.1$) very quickly. Blue upper triangles (theory) and green lower triangles (experiment) show such a case. In addition, we notice that when the step of QW $n \geq 4$, it is clearly to distinguish between cases with and without bound states.

The above experiments illustrate that the existence of bound states in the inhomogeneous 2D QW does not depend on Chern numbers or the bulk-boundary correspondence theorem. The observation of bound states in the inhomogeneous 2D QW requires the system to cross gapless phases when changing continuously from $(\theta_1, \theta_{2,+})$ to $(\theta_1, \theta_{2,-})$. Similar phenomena have been theoretically analyzed in Ref. [38]. Furthermore, such bound states have the topological origin. In the following we test the robustness of these bound states against small perturbations and disorder.

We introduce the small variation of rotation angles with the case in Fig. 3(c), which is indicated as brown circles in Fig. 4(b). Figure 4(c) displays the corresponding experimental probability distribution at the fourth step. Probability distributions for other steps ($n \leq 3$) are provided in Sec. SVI of the Supplemental Material [48]. We find that the localized probability along the boundary always appears when the rotation angle varies without crossing gapless phases. From the inset of Fig. 4(c), we find that bound states along the boundary appear. If we change

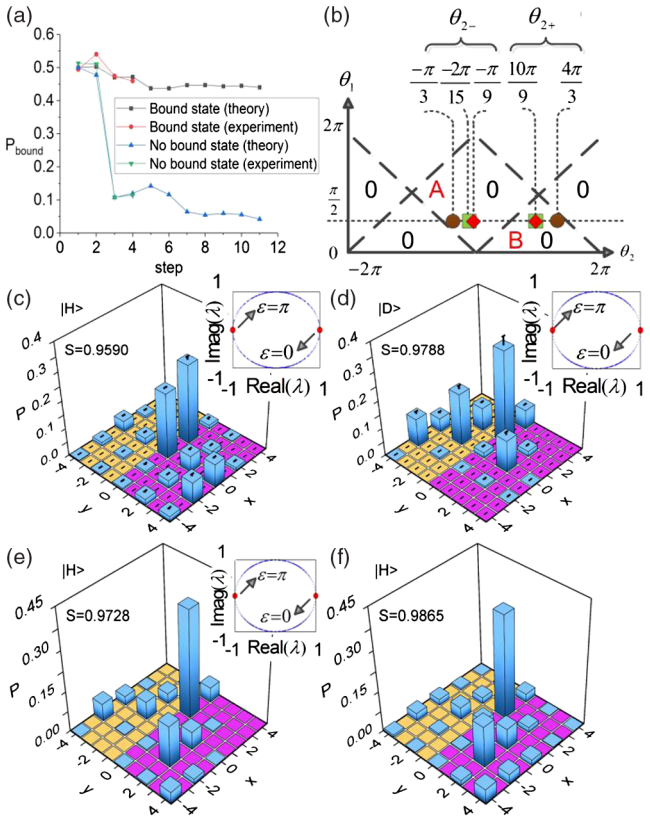

FIG. 4. (a) The localized probability P_{bound} at the boundary in 2D QWs with step. The cases with and without bound states are obviously different with the step $n \geq 4$. (b) The phase diagram for the 2D QW. Brown circles, green squares and red diamonds are coin rotations in (c),(d), and (e). (c)–(d) Bound states are robust against small perturbations. (c) Measured probability distribution at the fourth step with rotation angles changing from the case in Fig. 3(c) to $(\theta_1 = (\pi/2),\ \theta_{2,-} = -(\pi/3))$ and $(\theta_1 = (\pi/2),\ \theta_{2,+} = (4\pi/3))$. (d) Measured probability distribution at the fourth step with initial polarization changing to $|D\rangle$. Error bars indicate the standard deviation. Insets in (c) and (d), the eigenvalues $\lambda = e^{-i\varepsilon}$ of U, red dots indicate bound states. (e)–(f) Bound states are robust against disorder. Measured probability distributions at the fourth step without (e) and with (f) disorder. (e) Parameters are $(\theta_1 = (\pi/2),\ \theta_{2,-} = -(\pi/9))$ and $(\theta_1 = (\pi/2),\ \theta_{2,+} = (10/9)\pi)$; inset, the eigenvalues $\lambda = e^{-i\varepsilon}$ of U, red dots indicate bound states. (f) Compared with the case in (e), the disorder is introduced to $\theta_{2\pm} + \delta\theta$, where $\delta\theta$ is chosen uniformly from the intervals $[-(2\pi/9), (2\pi/9)]$.

the initial polarization to $|D\rangle$, in Fig. 4(d), we find that localized probabilities at the boundary emerge and bound states still exist. That is to say, these bound states are robust against small perturbations in 2D QWs. Furthermore, in order to test the robustness of topologically bound states against the disorder, we randomly generate ten sets of coin rotations and provide the mean values of probabilities at the fourth step in Fig. 4(f). Comparing the probability distributions in Figs. 4(f) and 4(e), we find that the measured probability distributions with the disorder [Fig. 4(f)] are

highly similar to those without the disorder [Fig. 4(e)], which demonstrate the robustness of bound states against the disorder.

In summary, we have constructed a new 2D QW experimental platform using spatial positions and OAM of light. The advantage of full control of each lattice site in the 2D QW makes our experimental platform suitable for topological study. We have observed 2D topological edge states with vanishing Chern numbers and confirmed the robustness of these edge states against small perturbations and disorder. Such a phenomenon goes beyond what has been known in static systems and is unique to periodically driven systems. In addition, our experimental setup can also be used as a powerful platform to study other topics including energy transport in the 2D QW and so on [38,39,49–51]. Furthermore, our construction opens up a new avenue to implement high-dimensional QWs in the experiment, which are prerequisites to realize quantum search algorithms [52,53].

This work was supported by the National Key Research and Development Program of China under Grant No. 2017YFA0303800 and the National Natural Science Foundation of China (11574031 and 11604014).

Note added.—Recently, we have noticed that topologically protected edge states in a 2D QW have been also experimentally observed in a fiber-loop architecture [54].

*These authors contributed equally to this work.
‡To whom correspondence should be addressed. zhangxd@bit.edu.cn
†To whom correspondence should be addressed. chentian@bit.edu.cn

[1] C. Nayak, S. H. Simon, A. Stern, M. Freedman, and S. Das Sarma, Rev. Mod. Phys. **80**, 1083 (2008).
[2] M. Z. Hasan and C. L. Kane, Rev. Mod. Phys. **82**, 3045 (2010).
[3] X.-L. Qi and S.-C. Zhang, Rev. Mod. Phys. **83**, 1057 (2011).
[4] J. Dalibard, F. Gerbier, G. Juzeliūnas, and P. Öhberg, Rev. Mod. Phys. **83**, 1523 (2011).
[5] S.-Y. Lin, E. Chow, V. Hietala, P. R. Villeneuve, and J. D. Joannopoulos, Science **282**, 274 (1998).
[6] S. D. Huber, Nat. Phys. **12**, 621 (2016).
[7] F. D. M. Haldane, Phys. Rev. Lett. **61**, 2015 (1988).
[8] C. L. Kane and E. J. Mele, Phys. Rev. Lett. **95**, 146802 (2005).
[9] M. König, S. Wiedmann, C. Brüne, A. Roth, H. Buhmann, L. W. Molenkamp, X.-L. Qi, and S.-C. Zhang, Science **318**, 766 (2007).
[10] D. Hsieh, D. Qian, L. Wray, Y. Xia, Y. S. Hor, R. J. Cava, and M. Z. Hasan, Nature (London) **452**, 970 (2008).
[11] A. Das, Y. Ronen, Y. Most, Y. Oreg, M. Heiblum, and H. Shtrikman, Nat. Phys. **8**, 887 (2012).
[12] D. J. Thouless, M. Kohmoto, M. P. Nightingale, and M. den Nijs, Phys. Rev. Lett. **49**, 405 (1982).
[13] A. P. Schnyder, S. Ryu, A. Furusaki, and A. W. W. Ludwig, Phys. Rev. B **78**, 195125 (2008).
[14] W. Hu, J. C. Pillay, K. Wu, M. Pasek, P. P. Shum, and Y. D. Chong, Phys. Rev. X **5**, 011012 (2015).
[15] F. Gao, Z. Gao, X. Shi, Z. Yang, X. Lin, H. Xu, J. D. Joannopoulos, M. Soljačić, H. Chen, L. Lu, Y. Chong, and B. Zhang, Nat. Commun. **7**, 11619 (2016).
[16] M. S. Rudner, N. H. Lindner, E. Berg, and M. Levin, Phys. Rev. X **3**, 031005 (2013).
[17] S. Mukherjee, A. Spracklen, M. Valiente, E. Andersson, P. Öhberg, N. Goldman, and R. R. Thomson, Nat. Commun. **8**, 13918 (2017).
[18] L. J. Maczewsky, J. M. Zeuner, S. Nolte, and A. Szameit, Nat. Commun. **8**, 13756 (2017).
[19] T. Ozawa *et al.*, arXiv:1802.04173v1.
[20] A. B. Khanikaev and G. Shvets, Nat. Photonics **11**, 763 (2017).
[21] E. Farhi and S. Gutmann, Phys. Rev. A **58**, 915 (1998).
[22] Y. Aharonov, L. Davidovich, and N. Zagury, Phys. Rev. A **48**, 1687 (1993).
[23] J. Kempe, Contemp. Phys. **44**, 307 (2003).
[24] S. E. Venegas-Andraca, Quantum Inf. Process. **11**, 1015 (2012).
[25] T. Kitagawa, M. S. Rudner, E. Berg, and E. Demler, Phys. Rev. A **82**, 033429 (2010).
[26] T. Kitagawa, M. A. Broome, A. Fedrizzi, M. S. Rudner, E. Berg, I. Kassal, A. Aspuru-Guzik, E. Demler, and A. G. White, Nat. Commun. **3**, 882 (2012).
[27] J. K. Asbóth and H. Obuse, Phys. Rev. B **88**, 121406(R) (2013).
[28] F. Cardano, F. Massa, H. Qassim, E. Karimi, S. Slussarenko, D. Paparo, C. de Lisio, F. Sciarrino, E. Santamato, R. W. Boyd, and L. Marrucci, Sci. Adv. **1**, e1500087 (2015).
[29] H. Obuse, J. K. Asbóth, Y. Nishimura, and N. Kawakami, Phys. Rev. B **92**, 045424 (2015).
[30] T. Chen, B. Wang, and X. Zhang, New J. Phys. **19**, 113049 (2017).
[31] F. Cardano, M. Maffei, F. Massa, B. Piccirillo, C. de Lisio, G. De Filippis, V. Cataudella, E. Santamato, and L. Marrucci, Nat. Commun. **7**, 11439 (2016).
[32] F. Cardano, A. D'Errico, A. Dauphin, M. Maffei, B. Piccirillo, C. de Lisio, G. De Filippis, V. Cataudella, E. Santamato, L. Marrucci, M. Lewenstein, and P. Massignan, Nat. Commun. **8**, 15516 (2017).
[33] V. V. Ramasesh, E. Flurin, M. Rudner, I. Siddiqi, and N. Y. Yao, Phys. Rev. Lett. **118**, 130501 (2017).
[34] E. Flurin, V. V. Ramasesh, S. Hacohen-Gourgy, L. S. Martin, N. Y. Yao, and I. Siddiqi, Phys. Rev. X **7**, 031023 (2017).
[35] T. Rakovszky, J. K. Asbóth, and A. Alberti, Phys. Rev. B **95**, 201407(R) (2017).
[36] X. Zhan, L. Xiao, Z. Bian, K. Wang, X. Qiu, B. C. Sanders, W. Yi, and P. Xue, Phys. Rev. Lett. **119**, 130501 (2017).
[37] L. Xiao, X. Zhan, Z. H. Bian, K. K. Wang, X. Zhang, X. P. Wang, J. Li, K. Mochizuki, D. Kim, N. Kawakami, W. Yi, H. Obuse, B. C. Sanders, and P. Xue, Nat. Phys. **13**, 1117 (2017).
[38] T. Kitagawa, Quantum Inf. Process. **11**, 1107 (2012).
[39] J. K. Asboth and J. M. Edge, Phys. Rev. A **91**, 022324 (2015).

[40] A. Schreiber, A. Gábris, P. P. Rohde, K. Laiho, M. Štefaňák, V. Potoček, C. Hamilton, I. Jex, and C. Silberhorn, Science **336**, 55 (2012).
[41] Y.-C. Jeong, C. Di Franco, H.-T. Lim, M. S. Kim, and Y.-H. Kim, Nat. Commun. **4**, 2471 (2013).
[42] K. Manouchehri and J. Wang, *Physical Implementation of Quantum Walks* (Springer Publishing Company, New York, 2013).
[43] S. Barkhofen, T. Nitsche, F. Elster, L. Lorz, A. Gábris, I. Jex, and C. Silberhorn, Phys. Rev. A **96**, 033846 (2017).
[44] K. Poulios, R. Keil, D. Fry, J. D. A. Meinecke, J. C. F. Matthews, A. Politi, M. Lobino, M. Gräfe, M. Heinrich, S. Nolte, A. Szameit, and J. L. O'Brien, Phys. Rev. Lett. **112**, 143604 (2014).
[45] S. K. Goyal, F. S. Roux, A. Forbes, and T. Konrad, Phys. Rev. Lett. **110**, 263602 (2013).
[46] M. A. Broome, A. Fedrizzi, B. P. Lanyon, I. Kassal, A. Aspuru-Guzik, and A. G. White, Phys. Rev. Lett. **104**, 153602 (2010).
[47] P. Xue, H. Qin, and B. Tang, Sci. Rep. **4**, 4825 (2014).
[48] See Supplemental Material at http://link.aps.org/supplemental/10.1103/PhysRevLett.121.100501 for detailed descriptions of the experimental implementation, observations of probability distributions with different steps and theoretical analysis of topological phases in the 2D QW.
[49] D. J. Thouless, Phys. Rev. B **27**, 6083 (1983).
[50] C. Di Franco, M. Mc Gettrick, and T. Busch, Phys. Rev. Lett. **106**, 080502 (2011).
[51] T. Chen and X. Zhang, Phys. Rev. A **94**, 012316(2016).
[52] A. Ambainis, J. Kempe, and A. Rivosh, in *Proceedings of the Sixteenth Annual ACM-SIAM Symposium on Discrete Algorithms* (Society for Industrial and Applied Mathematics, Philadelphia, PA, USA, 2005), p. 1099.
[53] N. Shenvi, J. Kempe, and K. B. Whaley, Phys. Rev. A **67**, 052307 (2003).
[54] C. Chen *et al.*, Phys. Rev. Lett., following Letter **121**, 100502 (2018).